

Misalignment errors in symmetric stereoscopic PIV systems

Nese*, F. G., Astarita, T. and Cardone, G.

*DETEC, University of Naples "Federico II"
p.le Tecchio, 80 – 80125 Naples, Italy
Tel. 0817683389 - Fax. 0812390364

Abstract

The main purpose of the present work is to estimate errors which occur in a symmetric stereoscopic system and which are caused by a misalignment between the calibration and the measurement planes. Analytical expressions as function of the flow displacement are derived for misalignment errors of the three displacement components. The error equations are derived for two different flow fields: a constant flow field in the measurement region and a spatially variable displacement field.

Errors due to a translation of the measurement plane with respect to the calibration plane as well as errors due to a relative rotation of the two planes are discussed in details. The effects of many parameters such as the distance between the cameras and the calibration target, the distance between the two cameras, the spatial coordinates in the measurement plane, the displacement gradient for each of the flow field components, the distance between the calibration and the measurement planes and the angles subtended by the coordinate system axes and the measurement plane are considered.

In order to test the validity of the equations found from theoretic considerations, experimental measurements have been conducted by using two angular stereoscopic system with Scheimpflug conditions: a warping method with a geometric reconstruction and a mapping method. No difference can be put in evidence from the errors computed with the two different methods. Measurements agree with the values computed by the reported formulas.

1. Introduction

At present stereoscopic particle image velocimetry (PIV) is the most widespread method which is used to conduct three-component PIV measurements on planar domains. All stereoscopic systems satisfy the requirement of recording two simultaneous but different views of the same object.

Commonly used stereoscopic systems can be classified according to translation systems and rotational systems. The latter require an additional rotation of the image plane with respect to the lens plane according to the Scheimpflug condition, in order to ensure that all the particles are in good focus in the image plane (see Prasad & Jensen, 1995 and Hinsch, 1995). Most stereoscopic DPIV systems employ calibration-based reconstructions which require the placement of a target in the object plane. The calibration-based methods can be classified into 2-d and 3-d methods. The former, such as the ones used by van Oord (1997) and by Willert (1997), employ a mapping function to relate the two-dimensional image plane to the two-dimensional object plane and combine the apparent displacements seen by each camera, using knowledge of the system geometry to reconstruct. The latter, such as the method used by Soloff et al. (1997), does not require knowledge of the system geometry at any stage during reconstruction, since the mapping function provides a direct relationship between a particle location in the neighbourhood of the object plane and its corresponding position on each image plane. A review of stereoscopic PIV measurements on planar domains can be found in Prasad (2000).

Error analyses have been presented by some authors for both translation and rotational systems. Arroyo & Greated (1991) and Prasad & Adrian (1993) have presented analyses for the former, while Lawson & Wu (1997) have presented standard error analyses for both systems, including the variation of error with off-axis position.

Another relevant source of error, which has not been widely investigated in the current litera-

ture, can be traced back to misalignments between the target plate and the laser sheet. As it has been reported by Willert (1997), for all the calibration-based methods it is crucial to ensure that the target plate during the calibration coincides exactly with the laser sheet during flow recording. In order to better understand the effect of misalignment errors on Stereoscopic PIV measurements, further investigations are required; therefore, in the present work, analytical expressions for a symmetric stereoscopic system are derived from geometric considerations and experimental investigations have been conducted. Only the main results will be reported in this paper: for complete derivations the reader is also advised to consult Nese (2004).

The paper is organized as follows. In §2 the theoretical expressions of the misalignment error are derived for both a constant and a spatially variable displacement field and for two different positions of the measurement plane. In §3 a brief discussion of the experimental apparatus and of the acquisition and image processing technique is presented. Experimental investigations and results are reported in §4, while conclusions are drawn in §5.

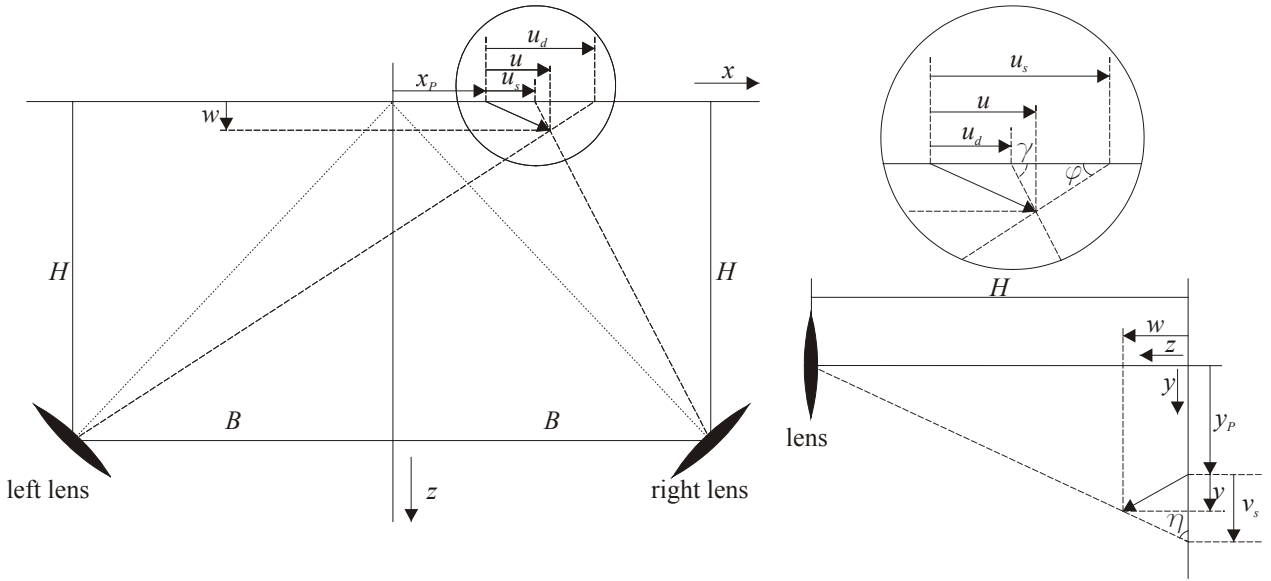


Figure 1. Schematic representation for the calculation of the three-dimensional displacements from the measured in-plane components by the two different cameras.

2. Theory

In order to evaluate errors due to misalignments, the reconstruction equations given in van Oord (1997) will be used:

$$u = \frac{B(u_s + u_d) + x_p(u_d - u_s)}{2B + u_s - u_d} \quad (1)$$

$$v = \frac{y_p(u_d - u_s) + 2Bv_s}{2B + u_s - u_d} = \frac{y_p(u_d - u_s) + 2Bv_d}{2B + u_s - u_d} \quad (2)$$

$$w = H \frac{u_s - u_d}{2B + u_s - u_d} \quad (3)$$

where H is the distance of the camera lenses from the measurement plane and B is half the distance between the two cameras. (u_s, v_s) and (u_d, v_d) are the components of the 2D warped vector respectively for left and right cameras (see Figure 1). The point P in the light sheet at which the displacement vector is to be determined has physical coordinates $(x_p, y_p, 0)$.

The expressions of the warped vectors as function of the true displacement can be found by solving the system of equations (1)-(3):

$$u_s = \frac{Hu + w(B + x_p)}{H - w} \quad (4)$$

$$u_d = \frac{Hu - w(B - x_P)}{H - w} \quad (5)$$

$$v_s = v_d = \frac{Hv + y_P w}{H - w}. \quad (6)$$

2.1. Uniform displacement

In this sub-section we will first analyse misalignment errors due to a z -axis translation of the laser sheet. Therefore, let the measurement plane π' be translated by $-\Delta z$ with respect to the calibration plane π and let P be a location of the target plane. Owing to the z -translation, the displacement corresponding to the point P' in the laser sheet is projected onto the left camera image plane (Figure 2). Since the measured vectors are back-projected in the object plane according to the “warping function” of the plane π , the true warped x -component of the displacement for the left camera u_s'' is smaller than both the projections at locations P and P' , denoted respectively with u_s and u_s' . If we assume that the displacement vectors at location P and location P' are the same, it is not difficult to obtain the actual component u_s'' .

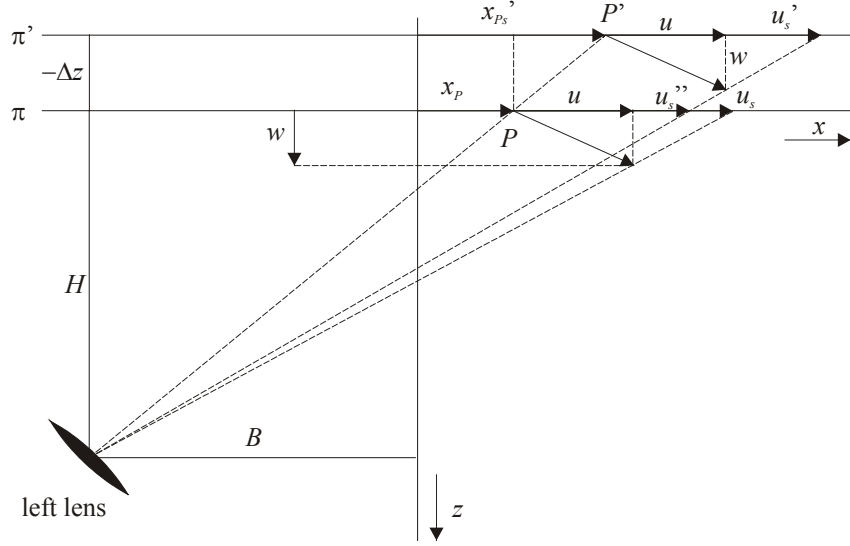


Figure 2 Schematic representation for the calculation of the true measured x -component by the left camera for a z -axis translation.

With reference to Figure 2, the following relationships can be found using simple geometry:

$$\frac{x'_{Ps} - x_P}{-\Delta z} = \frac{B + x_P}{H} \quad (7)$$

$$\frac{B + x'_{Ps} + u'_s}{H - \Delta z} = \frac{u'_s - u}{w} = \frac{B + x_P + u''_s}{H}. \quad (8)$$

Solving equations (7) and (8) for x'_{Ps} and u_s'' gives:

$$x'_{Ps} = x_P - \Delta z \frac{(B + x_P)}{H} \quad (9)$$

$$u''_s = \frac{Hu + w(B + x_P)}{H - \Delta z - w}. \quad (10)$$

Using equation (4), the latter can be rewritten in a form which will be useful in the remainder of the paper:

$$u''_s = u_s \left(1 + \frac{\Delta z}{H - w - \Delta z} \right). \quad (11)$$

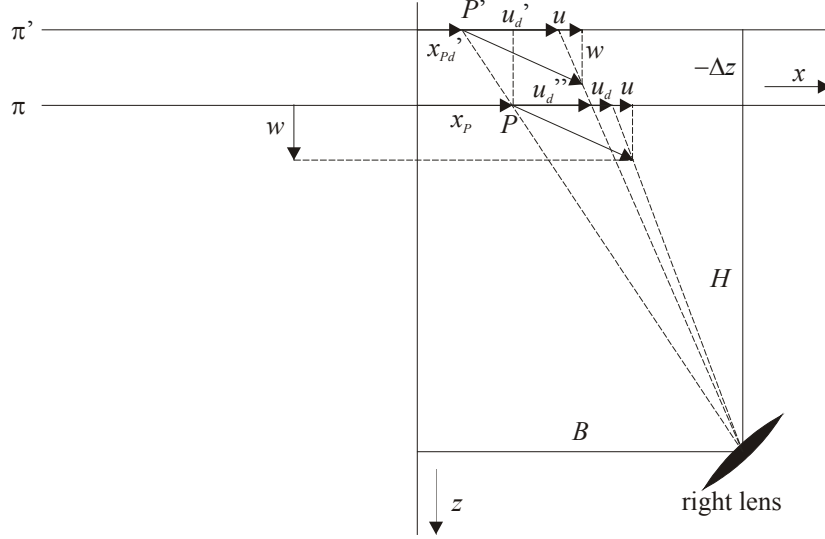


Figure 3 Schematic representation for the calculation of the true measured x -component by the right camera for a z -axis translation.

By analogy with (9) and (10) respectively, for the right camera one obtains (Figure 3):

$$x'_{Pd} = x_p + \Delta z \frac{(B - x_p)}{H} \quad (12)$$

$$u_d'' = \frac{Hu - w(B - x_p)}{H - \Delta z - w}. \quad (13)$$

Equation (13) can also be written in the form:

$$u_d'' = u_d \left(1 + \frac{\Delta z}{H - w - \Delta z} \right). \quad (14)$$

Substitution of (10) and (13) in (1) and (3) respectively yields:

$$u' = \frac{Hu}{H - \Delta z} \quad (15)$$

and

$$w' = \frac{Hw}{H - \Delta z} \quad (16)$$

which constitute the actual velocity component measured by the stereoscopic system along the x and z -axis respectively. Therefore the misalignment errors, in terms of relative errors ε_u and ε_w , are given by:

$$\varepsilon_u = \frac{u' - u}{u} = \frac{\Delta z}{H - \Delta z} \quad (17)$$

$$\varepsilon_w = \frac{w' - w}{w} = \frac{\Delta z}{H - \Delta z}. \quad (18)$$

With reference to Figure 4 the actual velocity component along the y -axis can be obtained in the same way as shown for u and w components. Thus, by analogy with (12), (13), (14), (15) and (17) the resulting equations reduce to:

$$y'_{Pd} = y'_{Ps} = y_p - \frac{\Delta z}{H} y_p \quad (19)$$

$$v_d'' = v_s'' = \frac{Hv + y_p w}{H - \Delta z - w} \quad (20)$$

$$v_s'' = v_s \left(1 + \frac{\Delta z}{H - \Delta z - w} \right) \quad (21)$$

$$v' = \frac{-2y_p w B + 2BHv + 2By_p w}{2B(H - \Delta z - w) + 2wB} = \frac{Hv}{H - \Delta z} \quad (22)$$

$$\varepsilon_v = \frac{v' - v}{v} = \frac{\Delta z}{H - \Delta z}. \quad (23)$$

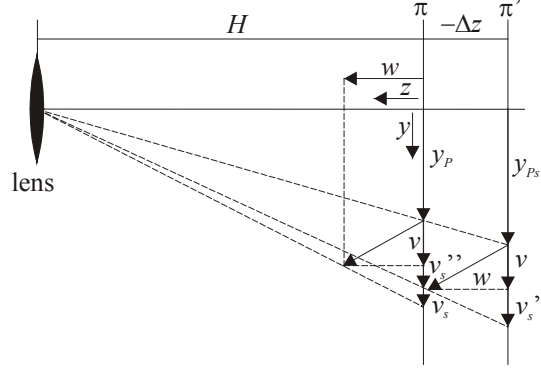


Figure 4 Schematic representation for the calculation of the true measured y -component by the left (right) camera for a z -axis translation.

Note that the relative error is identical for all the displacement components and it depends only on the z -axis translation and on the distance of the cameras from the calibration target. Furthermore, for a typical laboratory configuration, the field of view is imaged at an object distance of 400mm with a translation of the light sheet which is less than 4mm ; hence, misalignment errors of less than 1% of the true displacement components are incurred. Obviously, these errors decrease for increasing H .

When the light sheet is tilted about the y -axis, the error equations are not as simple as those derived for a z -axis translation because of the geometric asymmetry of the configuration. As it can be seen from Figure 5, quantity Δz is not constant along the x -axis and at location P in the target plane, for the left camera, it is given by:

$$\Delta z_s = \frac{H \operatorname{tg} \alpha (x_p - x_c)}{(x_p + B) \operatorname{tg} \alpha - H}. \quad (24)$$

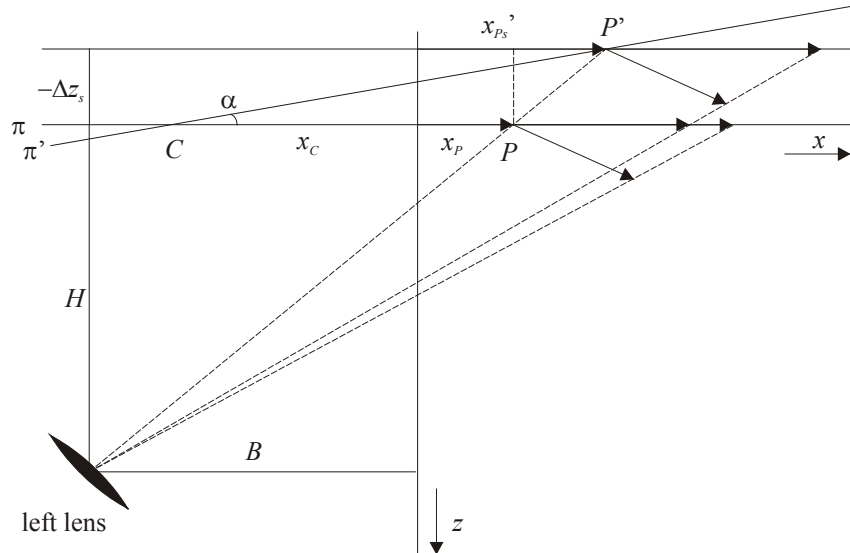


Figure 5 Schematic representation for the calculation of the true measured x -component by the left camera for a tilt angle α about the centre of rotation C in the $y=0$ plane.

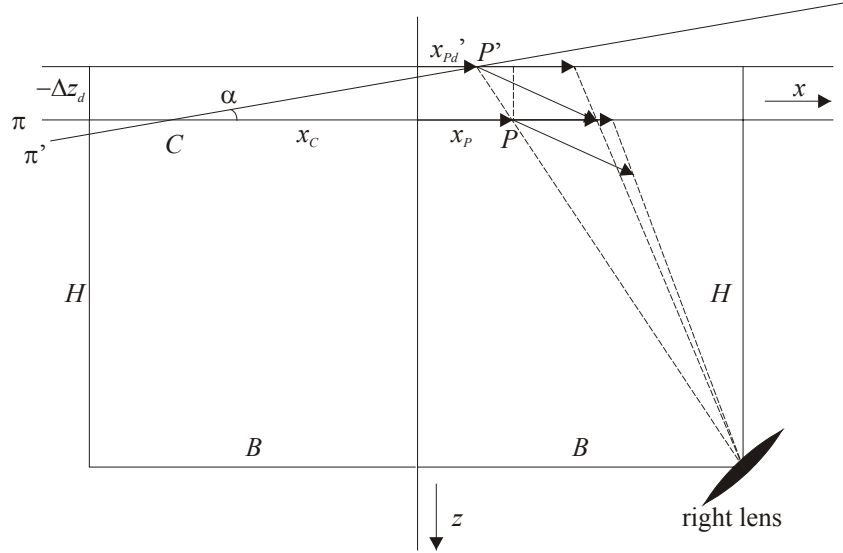


Figure 6 Schematic representation for the calculation of the actual measured components by the right camera for a tilt angle α about the centre of rotation C in the $y=0$ plane.

Owing to the aforementioned asymmetry, quantity Δz for the right camera is different from that which is seen from the left camera. For the right camera relationship (24) reduces to (see Figure 6):

$$\Delta z_d = \frac{H(x_p - x_c) \operatorname{tg} \alpha}{(x_p - B) \operatorname{tg} \alpha - H}. \quad (25)$$

Subscripts s and d in (24) and (25) refer to left and right cameras respectively while α represents the angle enclosed by the target plane and the light sheet. Because of this difference, the relative error expressions are not as simple as (17), (18) and (23). If we define coefficients f_s and f_d as:

$$f_s = \frac{\Delta z_s}{H - w - \Delta z_s}, \quad f_d = \frac{\Delta z_d}{H - w - \Delta z_d} \quad (26)$$

we can rewrite the 2D warped components as:

$$u_s'' = u_s(1 + f_s), \quad u_d'' = u_d(1 + f_d), \quad v_s'' = v_s(1 + f_s) \quad \text{e} \quad v_d'' = v_d(1 + f_d). \quad (27)$$

By substitution of equations (27) in (1)-(3) we obtain the following expressions of the relative errors in terms of coefficients (26):

$$\varepsilon_u = \frac{1}{u} \frac{Bu(H-w)(f_s + f_d) - [(Hu + wx_p)(u + x_p) - wB^2](f_s - f_d)}{2BH + wB(f_s + f_d) + (Hu + wx_p)(f_s - f_d)} \quad (28)$$

$$\varepsilon_v = \frac{1}{v} \frac{Bv(H-w)(f_s + f_d) - (v + y_p)(Hu + wx_p)(f_s - f_d)}{2BH + wB(f_s + f_d) + (Hu + wx_p)(f_s - f_d)} \quad (29)$$

$$\varepsilon_w = \frac{H-w}{w} \frac{Bw(f_s + f_d) + (Hu + wx_p)(f_s - f_d)}{2BH + wB(f_s + f_d) + (Hu + wx_p)(f_s - f_d)}. \quad (30)$$

Equations reported above show that the misalignment errors consist of two terms: a symmetric one which is given by the sum of the (26) and an asymmetric one which is related to the difference of the two coefficients. By considering the definition of coefficients (26), relationships (28)-(30) can be written as:

$$\varepsilon_u = \frac{(H-w)(x_p - x_c) \operatorname{tg} \alpha}{u} \frac{Hu[w - H + (x_c + u + x_p) \operatorname{tg} \alpha] + w(x_p^2 - B^2) \operatorname{tg} \alpha}{D_1^2 - D_2} \quad (31)$$

$$\varepsilon_v = \frac{(H-w)(x_p - x_c) \operatorname{tg} \alpha}{v} \frac{Hv[w - H + (x_c + u) \operatorname{tg} \alpha] + y_p(Hu + wx_p) \operatorname{tg} \alpha}{D_1^2 - D_2} \quad (32)$$

$$\varepsilon_w = \frac{H(H-w)(x_p - x_c)tg\alpha w[w-H + (x_c - x_p + u)tg\alpha] - Hu tg\alpha}{w(D_1^2 - D_2)} \quad (33)$$

with

$$D_1 = H(H-w) + (wx_p - Hx_c)tg\alpha$$

and

$$D_2 = (H-w)^2 B^2 tg^2 \alpha - Htg\alpha(x_p - x_c)[w(w-H) + (wx_c - wx_p - Hu + uw)tg\alpha].$$

For small displacement components and tilt angles misalignment errors are identical for all the components and equations (31)-(33) reduce to:

$$\varepsilon_u = \varepsilon_v = \varepsilon_w = \frac{(x_c - x_p)}{H} tg\alpha. \quad (34)$$

For a typical laboratory configuration, if the tilt angle is smaller than 3° (34) is a good approximation of the actual misalignment error. In this case relative errors are also less than 1% of the measured displacement all over the image field of view.

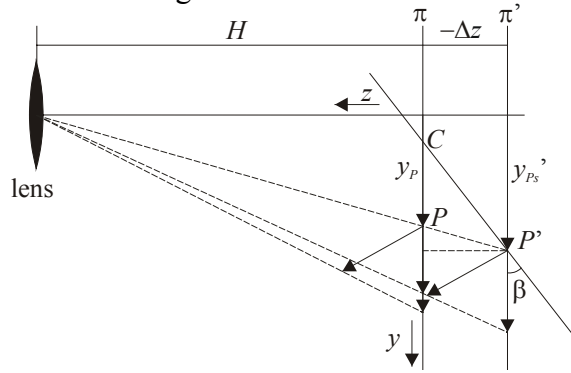


Figure 7 Schematic representation for the calculation of the actual measured components by the cameras for a tilt angle β about the centre of rotation C in the $x=0$ plane.

As shown in Figure 7 when the light sheet is tilted about the x -axis, even though it varies in x , quantity Δz is the same for both cameras and is given by:

$$\Delta z_s = \Delta z_d = \frac{H(y_p - y_c)tg\beta}{y_p tg\beta - H} \quad (35)$$

where β is the tilt angle. Because of the symmetry, substitution of (35) in (26) and subsequently in (28)-(30) will simply yield:

$$\varepsilon_u = \varepsilon_v = \varepsilon_w = \frac{(y_c - y_p)tg\beta}{H - y_c tg\beta}. \quad (36)$$

2.2. Spatially variable displacement field

Since the displacement vector is not uniform in the measurement plane, coefficients f_s and f_d are not equal for the horizontal and vertical warped components. Hence, (27) can be written in the form:

$$u_s'' = u_s(1 + f_s^u), u_d'' = u_d(1 + f_d^u), v_s'' = v_s(1 + f_s^v) \text{ e } v_d'' = v_d(1 + f_d^v). \quad (37)$$

With such definitions misalignment errors can be found by the following equations:

$$\varepsilon_u = \frac{1}{u} \frac{Bu(H-w)(f_s^u + f_d^u) - [(Hu + wx_p)(u + x_p) - wB^2](f_s^u - f_d^u)}{2BH + wB(f_s^u + f_d^u) + (Hu + wx_p)(f_s^u - f_d^u)} \quad (38)$$

$$\varepsilon_v = \frac{1}{v} \frac{B(Hv + y_p w)(f_s^v + f_d^v) - (v + y_p)(Hu + wx_p)(f_s^v - f_d^v) - wB(v + y_p)(f_s^v + f_d^v)}{2BH + wB(f_s^v + f_d^v) + (Hu + wx_p)(f_s^v - f_d^v)} \quad (39)$$

$$\varepsilon_w = \frac{H-w}{w} \frac{Bw(f_s^u + f_d^u) + (Hu + wx_p)(f_s^u - f_d^u)}{2BH + wB(f_s^u + f_d^u) + (Hu + wx_p)(f_s^u - f_d^u)} \quad (40)$$

where coefficients defined by (37) depend on the spatial displacement gradients which can be expressed in the form:

$$u_{es} = u(1 + f_{eus}), v_{es} = v(1 + f_{evs}), w_{es} = w(1 + f_{ews}) \quad (41)$$

$$u_{ed} = u(1 + f_{eud}), v_{ed} = v(1 + f_{evd}), w_{ed} = w(1 + f_{ewd}). \quad (42)$$

(u_{es}, v_{es}, w_{es}) and (u_{ed}, v_{ed}, w_{ed}) are the effective velocity components which are projected respectively onto the left and right cameras. By simple considerations the relationships between coefficients defined in (37) and those defined in (41) and (42) can be found:

$$f_s^u = \frac{1}{H - \Delta z_s - w - wf_{ews}} \left\{ \Delta z_s + \frac{H[uf_{eus}(H - w) + wf_{ews}(B + x_p + u)]}{Hu + w(B + x_p)} \right\} \quad (43)$$

$$f_d^u = \frac{1}{H - \Delta z_d - w - wf_{ewd}} \left\{ \Delta z_d + \frac{H[uf_{eud}(H - w) + wf_{ewd}(u - B + x_p)]}{Hu - w(B - x_p)} \right\} \quad (44)$$

$$f_s^v = \frac{1}{H - \Delta z_s - w - wf_{ews}} \left\{ \Delta z_s + \frac{H[vf_{evs}(H - w) + wf_{ews}(v + y_p)]}{Hv + y_p w} \right\} \quad (45)$$

$$f_d^v = \frac{1}{H - \Delta z_d - w - wf_{ewd}} \left\{ \Delta z_d + \frac{H[vf_{evd}(H - w) + wf_{ewd}(v + y_p)]}{Hv + y_p w} \right\}. \quad (46)$$

Note that coefficients $f_{eus}, f_{evs}, f_{ews}, f_{eud}, f_{evd}$ and f_{ewd} are related to the displacement field in the measurement region. In the following only expressions for a rotation about the centre of rotation C in the $y=0$ plane are given (see Figure 8):

$$f_{eus} = \Delta z_s \frac{(B + x_p)(1 - \cos \alpha) + H \sin \alpha}{H(x_c - x_p)(1 - \cos \alpha)}, f_{eud} = \Delta z_d \frac{(x_p - B)(1 - \cos \alpha) + H \sin \alpha}{H(x_c - x_p)(1 - \cos \alpha)} \quad (47)$$

$$f_{evs} = f_{evd} = 0 \quad (48)$$

$$f_{ews} = \Delta z_s \frac{(B + x_p) \sin \alpha - H(1 - \cos \alpha)}{H(x_c - x_p) \sin \alpha}, f_{ewd} = \Delta z_d \frac{(x_p - B) \sin \alpha - H(1 - \cos \alpha)}{H(x_c - x_p) \sin \alpha}. \quad (49)$$

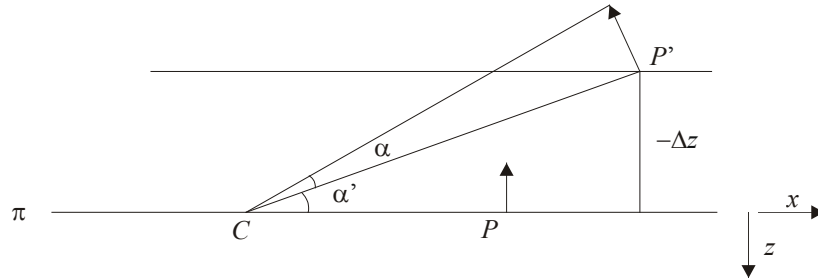


Figure 8 Schematic representation for the calculation of coefficients defined by (41) and (42) for a rotational displacement field of α about the centre C .

3. Set-up and processing

2D-3CPIV images are recorded with two CCD PCO-Sensicam cameras using an f-number of 2.8. The CCD sensor consists of 1280×1024 pixels with a physical dimension of $6.7 \times 6.7 \mu m^2$. Each image is digitised at 12 bits, so that a rather high number of grey levels (4096) may be used. The calibration target used in the experiments was a paper of black dots arranged on a uniform 30×30 Cartesian grid and stuck onto a rectangular plate. The centre-to-centre spacing of the circles was 5 mm in x and y . A computer generated pattern of particles mounted on rotation and translation stages is used to set reference displacements and misalignments of the measurement plane. As determined by the resolution of the mechanical indicators, the uncertainty in the displacement was $\pm 5 \mu m$, while the uncertainty in the rotation was $\pm 1^\circ$.

Two stereoscopic methods are used to measure the velocity vectors: a 3-d method proposed by Soloff et al. (1997) and a 2-d method which is similar to the one proposed by van Oord (1997).

Instead of interrogating the particle image first, the implemented 2-d method directly maps the recorded images to the object plane and performs the interrogation on the final Cartesian grid. The rms error in the mapping function was calculated to be about 0.40 pixels for both cameras. The PIV interrogation process is standard. The cross-correlation of the two interrogation images is evaluated by using the classical FFT and the displacement is determined at sub-pixel level by a Gaussian peak fit. An iterative procedure is used to perform a translation, a rotation and a deformation of the interrogation windows and to refine the size of the interrogation areas. The starting and final interrogation areas consist of 64×64 and 32×32 pixels respectively with an overlap of 50% and a distance of 0.5 mm between two adjacent vectors. Spurious vectors are detected with an automated data validation criterion at each intermediate step of the iteration process. Outliers are discarded and replaced with values calculated by a bilinear interpolation of nearby vectors.

4. Results

In this section the experimental error analysis is presented for both uniform and spatially variable displacements. All the results are reported in terms of absolute errors since in some cases the measured displacement components approach or even equal zero. Henceforth the absolute errors in u , v and w will be denoted by e_u , e_v and e_w respectively.

4.1. Uniform displacement

Figure 9 shows the misalignment error in u for a uniform displacement of $u = v = w = 0.4$ mm and a z -axis translation of 2 mm. As it can be seen from the figure, the experimental error is about constant in the measurement plane and the deviation of the experimental results from the theoretical predictions is below the uncertainty in the pattern displacement. Errors in v and w show similar trends to that reported in Figure 9 and therefore they are not analysed. The uncertainty in the out-of-plane component is slightly greater than errors in the in-plane components because camera angles of the present experimental set-up are less than 45° .

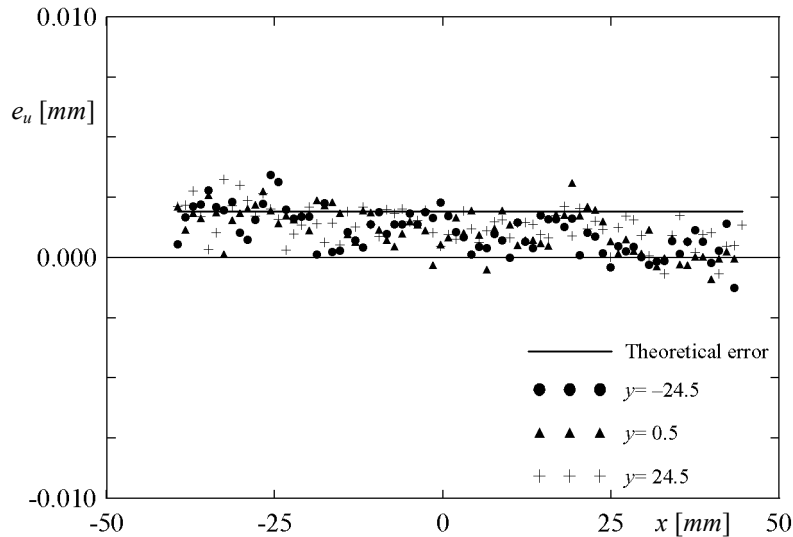


Figure 9 Variation of error in u displacement with x -axis for a z -axis translation of 2mm and a uniform displacement $u = v = w = 0.4$ mm. The theoretical error is plotted in continuous line. Symbols denote experimental errors at different y in the object plane.

Errors for a tilt about the y -axis are below experimental uncertainties as well and, in agreement with (34), they are about the same for all the displacement components. In Figure 10, for instance, error in v component versus x -axis is plotted for a uniform displacement $u = v = w = -0.4$ mm and a tilt angle of -1° . Results are reported for both tested stereoscopic systems and no relevant difference can be noted between the two methods. Only slightly higher fluctuations in the experimental trends are found for the 2d-Method.

Figure 11 shows variation of error e_w with x -axis for $u = v = w = 0.4$ mm and a tilt angle of 2° .

Also under these conditions the experimental trends match the theoretical predictions well and e_w seems to be more sensitive to variations of geometrical parameters.

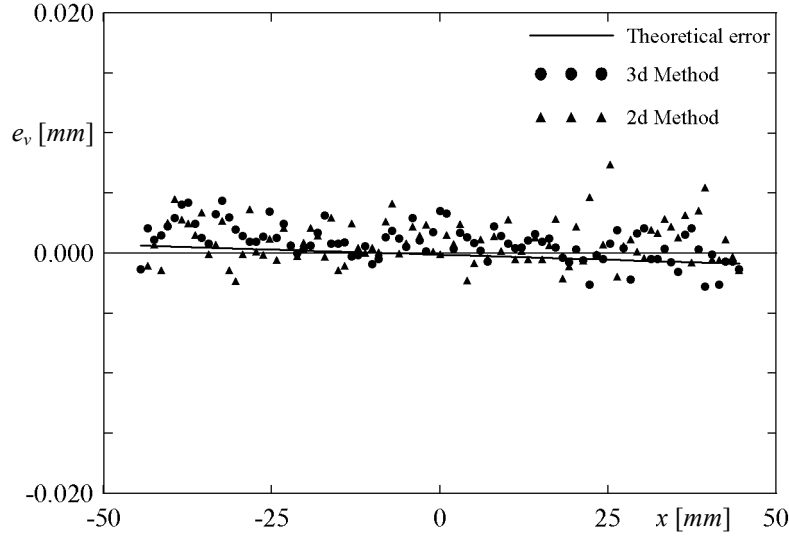


Figure 10 Variation of error in v displacement with x -axis for a y -axis tilt angle of -1° and a uniform displacement $u = v = w = -0.4 \text{ mm}$. The theoretical error is plotted in continuous line. Black circles denote experimental errors as measured with the 3d method; black triangles denote experimental errors as measured with the 2d method.

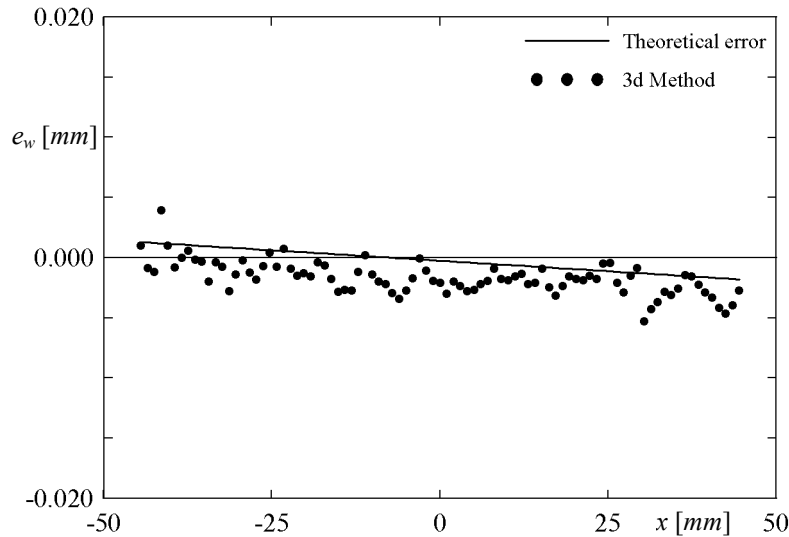


Figure 11 Variation of error in w displacement with x -axis for a y -axis tilt angle of 2° and a uniform displacement $u = v = w = 0.4 \text{ mm}$. The theoretical error is plotted in continuous line. Black circles denote experimental errors as measured with the 3d method.

4.2. Rigid rotation

In section 2.2 it was stated that for a spatially variable displacement misalignment errors are quite higher than those found for a uniform velocity field. Under these conditions, actual errors in the displacement components are related to the peculiar characteristics of the flow field. In the present work only the displacement field due to a rigid rotation around the y -axis has been tested. For such gradients only the x component shows high errors and therefore only e_u will be presented in the following figures. However, it should be noted that, owing to the values of camera angles and to the measurement procedure, the variance in the w component is quite high; as a consequence, the e_w error occasionally does not match the theoretical prediction and, in order to have reliable results an ensemble average operation over a higher number of measurements should be done.

In Figure 12 variation of e_u with x -axis for a z -axis translation of -1 mm and for a rigid rotation of -1° is plotted at ordinate $y = -24.5 \text{ mm}$. Measured errors with both methods are in agree-

ment with the theoretical curve, the maximum difference being lower than $5\mu\text{m}$. As it could be found analytically by equations derived in section 2, e_u is almost constant across the imaging field of view.

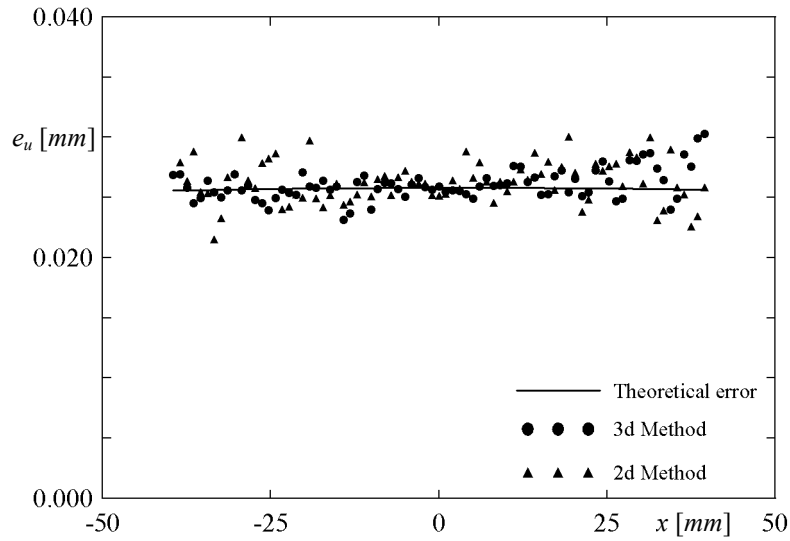


Figure 12 Variation of error in u displacement with x -axis for a z -axis translation of -1 mm and for a rigid rotation of -1° around the y -axis. The theoretical error is plotted in continuous line. Black circles denote experimental errors as measured with the 3d method; black triangles denote experimental errors as measured with the 2d method.

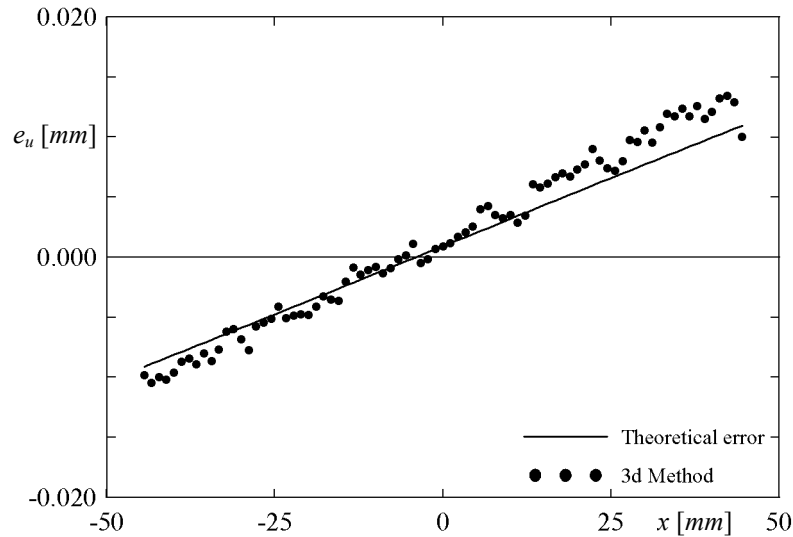


Figure 13 Variation of error in u displacement with x -axis for a y -axis tilt angle of 0.5° and for a rigid rotation of 1° around the y -axis. The theoretical error is plotted in continuous line. Black circles denote experimental errors as measured with the 3d method.

Considering a rotation of the measurement plane, the absolute error is linear with x -direction for the adopted geometric configuration. This is clearly seen in Figure 13 where e_u is plotted for a rigid rotation of 1° around the y -axis and for a measurement plane tilt of 0.5° . A small deviation of the experimental results from the theoretical predictions is found away from the centre of rotation because of the aforementioned uncertainty in the rotational stages.

Results have also shown that the Misalignment errors increase with the tilt angle is nearly linear, as it is shown in Figure 14 in which quantity e_u is plotted versus x -axis for a tilt angle of 2° and a rigid rotation of -1° . In fact, under these conditions the slope of the line, which experimental data match, is four times that which has been shown in Figure 13. The reported results are ensemble averaged over three measurements in order to reduce noise and to evidence more clearly the experimental trends.

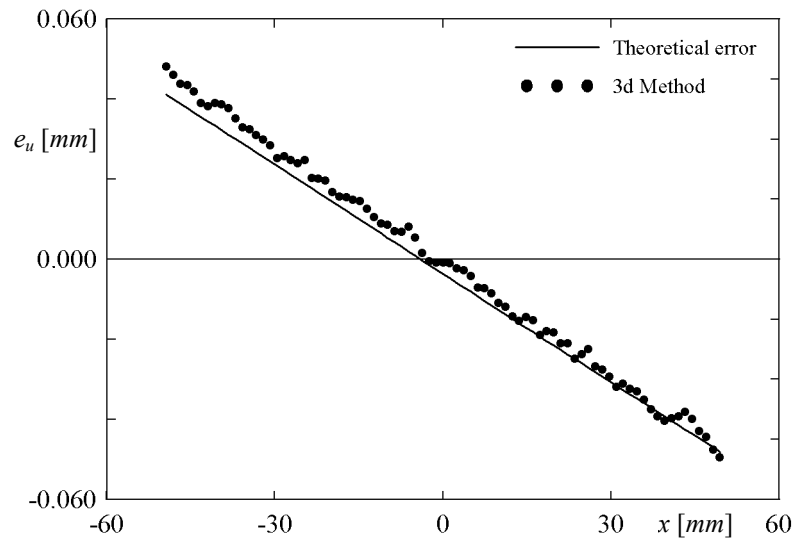


Figure 14 Variation of error in u displacement with x -axis for a y -axis tilt angle of 2° and for a rigid rotation of -1° around the y -axis. The theoretical error is plotted in continuous line. Black circles denote experimental errors as measured with the 3d method.

5. Conclusions

In the present work misalignment errors in symmetric stereoscopic PIV systems are analysed. Theoretical equations are derived for a translation and a rotation of the calibration target with respect to the laser light sheet plane.

As expected, for a uniform vector field in the measurement region, both errors are negligible while, for spatially variable displacement field, errors can reach up to 10-20% of the effective displacement. From a theoretical point of view, misalignment errors are found to be more sensitive to x -axis gradients.

Results evaluated from theoretic predictions are compared with experimental measurements carried out by means of translation and rotational stages. A uniform and a spatially variable vector have been tested. The latter has been generated by a rigid rotation of the target plane. Experimental data match the theoretical predictions in most cases. Only errors in w component in some cases show a high discrepancy because of the high variance which can be traced back to the value of the camera angles and to the measurement procedure. Furthermore the two stereoscopic methods, which have been used to measure the displacement field, have given nearly identical results.

REFERENCES

- ARROYO, M. P. & GREATED, C. A. 1991 *Stereoscopic particle image velocimetry*. Meas. Sci. Technol. 2, pp. 1181-1186.
- HINSCH, K., D. 1995 *Three-dimensional particle velocimetry*. Meas. Sci. Technol. 6, pp. 742-753.
- LAWSON, N. J. & WU, J. 1997 *Three-dimensional particle image velocimetry: error analysis of stereoscopic techniques*. Meas. Sci. Technol. 8, pp. 894-900.
- NESE, F. G. 2004 *Sviluppi nelle tecniche PIV stereoscopiche: errori di allineamento ed applicazioni allo studio termo-fluidodinamico di un getto che si immette in un flusso trasversale*. Tesi di dottorato, Università degli studi di Napoli "Federico II".
- OORD, J. VAN 1997 *The design of a stereoscopic DPIV system*. MEAH Report 161, Delft University of Technology.
- PRASAD, A. K. 2000 *Stereoscopic particle image velocimetry*. Exp. Fluids 29, pp. 103-116.
- PRASAD, A. K. & ADRIAN, R. J. 1993 *Stereoscopic particle image velocimetry applied to liquid flows*. Exp. Fluids 15, pp. 49-60.
- PRASAD, A. K. & JENSEN, K. 1995 *Scheimpflug stereocamera for particle image velocimetry in liquid flows*. Appl. Optics 34, pp. 7092-7099.
- SOLOFF, S. M., ADRIAN, R. J. & LIU, Z. C. 1997 *Distortion compensation for generalized stereo-*

scopic particle image velocimetry. Meas. Sci. Technol. 8, pp. 1441-1454.

WILLERT, C. 1997 *Stereoscopic digital particle image velocimetry for application in wind tunnel flows*. Meas. Sci. Technol. 8, pp. 1465-1479.